

Plasmonic nanogaps for broadband and large spontaneous emission rate enhancement

Anthony P. Edwards and Ali M. Adawi

Citation: *Journal of Applied Physics* **115**, 053101 (2014); doi: 10.1063/1.4864018

View online: <http://dx.doi.org/10.1063/1.4864018>

View Table of Contents: <http://scitation.aip.org/content/aip/journal/jap/115/5?ver=pdfcov>

Published by the *AIP Publishing*

Articles you may be interested in

[Plasmonic metal nanocubes for broadband light absorption enhancement in thin-film a-Si solar cells](#)

J. Appl. Phys. **115**, 124317 (2014); 10.1063/1.4869785

[Influence of film thickness and nanograting period on color-filter behaviors of plasmonic metal Ag films](#)

J. Appl. Phys. **115**, 113104 (2014); 10.1063/1.4869128

[Spontaneous emission and collection efficiency enhancement of single emitters in diamond via plasmonic cavities and gratings](#)

Appl. Phys. Lett. **103**, 161101 (2013); 10.1063/1.4817397

[The effect of plasmonic particles on solar absorption in vertically aligned silicon nanowire arrays](#)

Appl. Phys. Lett. **97**, 071110 (2010); 10.1063/1.3475484

[Multiple enhanced transmission bands through compound periodic array of rectangular holes](#)

J. Appl. Phys. **106**, 093108 (2009); 10.1063/1.3254248



Goodfellow

metals • ceramics • polymers
composites • compounds • glasses

Save 5% • Buy online
70,000 products • Fast shipping

Plasmonic nanogaps for broadband and large spontaneous emission rate enhancement

Anthony P. Edwards and Ali M. Adawi^{a)}

Department of Physics and Mathematics, University of Hull, Cottingham Road, Hull HU6 7RX, United Kingdom

(Received 14 November 2013; accepted 21 January 2014; published online 4 February 2014)

We present the optical properties of a plasmonic nanogap formed between a silver metallic nanoparticle and an extended silver film that shows a strong enhancement in the spontaneous emission rate over the whole visible range. In particular, we use three-dimensional finite difference time domain calculations to study the spontaneous emission rate and the quantum efficiency of an emitting material placed within the gap region as a function of the geometrical parameters of the plasmonic nanogap. Our calculations reveal that the enhancements in the total decay rate can be divided into two regions as a function of wavelength; region I spans the wavelength range from 350 nm to 500 nm and peaks at approximately at 400 nm. Region II covers the spectral range between 500 nm and 1000 nm. The enhancements in total decay rate in region I are mainly dominated by Ohmic losses by the metal, while the enhancements in total decay rate in region II are mainly dominated by radiative decay rate enhancements. Furthermore, our calculations show over 100 times enhancement in the spontaneous emission rate in region II. We combine this with quantum efficiency enhancements of almost 30 times from materials with low intrinsic quantum efficiencies and only a small reduction in efficiency from those with high intrinsic quantum efficiencies. All results appear easily achievable using realistic geometrical parameters and simple synthesis techniques. These results are attributed to the strong field confinements in the nanogap region. The structures are of high interest for both the fundamental understanding of light matter interactions under extreme electromagnetic field confinements and also potential applications in quantum optics and Raman spectroscopy. © 2014 AIP Publishing LLC. [<http://dx.doi.org/10.1063/1.4864018>]

I. INTRODUCTION

In recent years, controlling the spontaneous emission of an active emitter such as a single molecule or a quantum dot has attracted much attention because of its potential applications in the area of quantum optics and also as a subject of great fundamental interest.^{1–13} Quantitatively, the modifications in spontaneous emission rate for an optical resonator can be described through the Purcell factor¹⁴

$$F_P = \frac{\Gamma_T}{\Gamma_0} = \frac{3}{4\pi^2} \frac{Q}{V} \left(\frac{\lambda}{n}\right)^3, \quad (1)$$

here Γ_T is the modified emission rate, Γ_0 is the free space emission rate, Q is the quality factor of the optical resonator and it is a measure of the confinement lifetime of photons by the optical resonator, V is the mode volume of the resonator and is a measure of the spatial confinement of the optical field by the resonator, and n is the refractive index of the resonator medium. Here, it is also worth noting that the Purcell factor depends on both the magnitude and direction of the electromagnetic field associated with the optical resonator at the spectral and spatial position of the emitting dipole.¹⁵

Fundamentally, there are two main approaches to control the spontaneous emission of light; the first is using dielectric based resonators⁵ and the second is using

plasmonic nanostructures.^{1–3,6–12} The first approach focuses mainly on optimising the Q factor of the optical resonator, this provides a large Purcell factor over a very narrow bandwidth of ~ 0.01 nm–0.1 nm.^{5,16,17} However, for room temperature applications, optical emitters exhibit broad band emission width. For example, the spectral linewidth of single conjugated polymer molecules can range between 5 nm (Ref. 18) and 40 nm,¹⁹ the spectral linewidth for a single colloidal quantum dot is 15 nm (Ref. 1) and the linewidth of a nitrogen vacancy centre in a diamond nanocrystal is 100 nm.¹⁷ As a result, the coupling of a broad bandwidth emitter into a dielectric resonator is weak and predominantly controlled by the ability of the resonator to provide a small mode volume V . Theoretically, the minimum value for V is determined by the diffraction limit $V = (\frac{\lambda}{2n})^3$ and that corresponds to a maximum Purcell factor of $F_P = \frac{6}{\pi^2} Q_m$, where Q_m is the emitting material quality factor.¹⁵ However, achieving a diffraction limited dielectric optical resonator is not a trivial task. So far, microspheres,²⁰ micropillars,^{21,22} and photonic crystals²³ have provided mode volumes ranging between $1120(\frac{\lambda}{2n})^3 - 0.8(\frac{\lambda}{2n})^3$. Despite these achievements in dielectric optical resonators, the reduced mode volume associated with these cavities leads to non-directional radiation patterns and very poor free space input/output light coupling efficiency. This limits their use in many applications in nanophotonics.²⁴

Recently, plasmonic nanocavities²⁵ have emerged as attractive structures in which to achieve both a very small

^{a)}a.adawi@hull.ac.uk

mode volume $V \sim 0.03(\frac{\lambda}{2n})^3$ (Ref. 26) and also a high collection efficiency of up to 70%.¹¹ These superior properties of plasmonic nanocavities over dielectric optical resonators make them attractive approach to many nanophotonic applications such as room temperature single-photon nanosources²⁷ and room temperature nanolasers.^{28,29}

Several theoretical and experimental attempts to design and fabricate plasmonic nanocavities for the modification of the spontaneous emission rate at optical frequencies have been already considered. For example, Kuttge *et al.*³⁰ predicted a Purcell factor of 2000 from an Ag/SiO₂/Ag nanopillar with a Q factor of 32 and a mode volume of $0.0026(\frac{\lambda}{2n})^3$. Vesseur *et al.*⁶ used boundary-element-method (BEM) calculations to design V groove gold nanocavities for enhancing the spontaneous emission rate. Purcell factors above 2000 are predicted in the near infrared region from cavities of Q factor of 10–50 and mode volume of $0.006(\frac{\lambda}{2n})^3$. Chowdhury *et al.*³¹ used finite difference time domain (FDTD) calculations to investigate how fluorescence is modified in the presence of two silver nanoparticles of a dimer system, both as a function of the nanoparticle size and the separation between the two silver nanoparticles. They predicted over 5000-fold enhancements in the total radiated power. Experimentally, Muskens *et al.*³² demonstrated 5-fold enhancements in the emission rate of fluorescent dye molecules coupled into a gold dimer. Furthermore, Kinkhabwala *et al.*¹³ experimentally reported 1340 times enhancement in the fluorescence of a single molecule incorporated into a gold bowtie nanoantenna system. Kravets *et al.*³³ showed over 40-fold enhancements in the far field emission signal of an organic layer integrated into the surface of vertically aligned composite plasmonic nanostructures. Esteban *et al.*¹¹ designed a silver patch antenna for single photon applications, with almost 34 times enhancement in the total emission rate and 14 times enhancement in the radiative decay rate over the visible range. This yielded an overall quantum efficiency of 0.4 for the emitter-patch antenna system. Recently, Russell *et al.*⁷ demonstrated experimentally around 1000-fold enhancements in the radiative emission rate of an Alq₃ layer coupled to a nanogap formed between a silver nanowire and a silver substrate, a structure similar to those proposed by Esteban *et al.*¹¹ In spite of the importance of these studies, up to now there is no systematic study on how the geometrical parameters of these nanogaps affect the emission process and the quantum efficiency of an emitting dipole.

In this paper, we present systematic and detailed three-dimensional FDTD calculations on how the total decay rate Γ_T , the radiative decay rate Γ_{rad} , the nonradiative decay rate Γ_{nr} , and the quantum efficiency (emission probability) of an emitting dipole are modified in the presence of a plasmonic nanogap. The nanogap is formed between a spherical silver nanoparticle of diameter D and an extended silver film of thickness t separated by a gap of width d as illustrated in Fig. 1. In the simulations, we assumed the refractive index of the gap $n = 1.5$ mimicking an inert organic host matrix such as PMMA. Our particular motivation for this design is to create plasmonic nanogaps capable of enhancing the radiative decay rate Γ_{rad} of an organic molecule. Clearly, as most organic materials emit light at visible wavelengths, we aim to

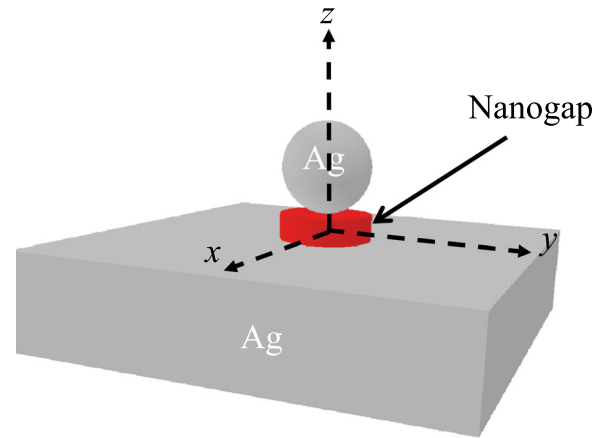


FIG. 1. A schematic drawing of the plasmonic nanogap investigated in this work.

enhance the radiative decay rate Γ_{rad} and suppress the nonradiative decay rate Γ_{nr} due to Ohmic losses over the whole visible range. The advantages of our proposed nanogaps over those used in other works are that our nanogaps do not require complicated and expensive fabrication techniques such as focused ion beam lithography or electron beam lithography. Simple chemical synthesis techniques can be used to synthesise the metallic nanoparticles in different shapes and size. The organic layer and the extended silver film can be fabricated by simple deposition techniques such as spin coating and thermal evaporation. A high degree of control over the nanogap width can be achieved by controlling the thickness of the organic layer d . This allows us to precisely control the relative contribution of Γ_{rad} and Γ_{nr} into the total decay rate Γ_T . This approach allowed us to achieve over 100 times enhancements in Γ_{rad} combined with emitter-nanogap system quantum efficiency ϕ_m in the range of 0.54–0.71 from organic molecules of intrinsic quantum efficiency ϕ_0 less than 0.7. The calculations indicated that over 100-fold enhancements in Γ_{rad} combined with $\phi_m \sim 0.71$ from organic molecules of intrinsic quantum efficiency in the range of 0.7–1 are achievable.

II. METHODS

The optical properties of the investigated nanogaps are simulated with a 3D FDTD method using the free available Meep software package³⁴ in which Maxwell's equations are rigorously solved. In our calculations, we followed the procedure proposed by Kaminski *et al.*³⁵ for calculating the decay rate components of an emitting dipole placed in the proximity of a metallic structure. In the calculations, the emitting molecule is represented by a classical dipole with an oscillating field in the z -direction and located at the gap centre (0,0,0) except if we specify otherwise. The normalised total decay rate $\frac{\Gamma_T}{\Gamma_0}$ and the normalised radiative decay rate $\frac{\Gamma_{rad}}{\Gamma_0}$ relative to the radiative decay rate of the emitting dipole in free space Γ_0 were computed by considering the relations³⁶

$$\frac{\Gamma_T}{\Gamma_0} = \frac{P_T}{P_0}, \quad \frac{\Gamma_{rad}}{\Gamma_0} = \frac{P_{rad}}{P_0}, \quad (2)$$

where P_0 is the power radiated by the emitting dipole in free space, P_T is the total power dissipated by the emitting dipole in the presence of the metal, and P_{rad} is the power radiated by the emitter-nanogap system. The nonradiative decay rate Γ_{nr} and the Purcell factor F_P can then be calculated via the relations $\Gamma_{nr} = \Gamma_T - \Gamma_{rad}$ and $F_P = \frac{\Gamma_T}{\Gamma_0}$, respectively. The quantum efficiency of the emitter-nanogap system ϕ_m can be written as

$$\phi_m = \frac{\Gamma_{rad}}{\Gamma_T + k_{nr}}, \quad (3)$$

where k_{nr} is the intrinsic nonradiative decay rate of the emitting dipole in free space. The quantum efficiency of the emitter-nanogap system ϕ_m can be related to the free space quantum efficiency $\phi_0 = \frac{\Gamma_0}{\Gamma_0 + k_{nr}}$ through the relation

$$\phi_m = \frac{\frac{\Gamma_{rad}}{\Gamma_0}}{\frac{\Gamma_T}{\Gamma_0} + \left(\frac{1}{\phi_0} - 1\right)}. \quad (4)$$

In all our calculations, we employed a grid spacing of 1 nm in each direction. Boundary conditions were implemented by introducing a perfect matching layer around the structure. In the simulations, we modelled the silver structures using a Lorentz-Drude model,³⁷ this incorporates the frequency-dependent effects of silver and other dispersive materials. Meep supports this through the form of a sum of harmonic resonances and a frequency independent term, all of which were modelled on well cited experimental optical constants.³⁸ As can be seen in Fig. 1, the nanogap is parameterised by three parameters; the diameter of the spherical silver nanoparticle D , the nanogap width d , and the thickness of the extended silver film t . In the calculations, we have varied D from 20 nm to 250 nm with 10 nm increments, d from 12 nm to 60 nm with 2 nm increments, and t from 30 nm to 250 nm.

III. RESULTS AND DISCUSSION

In order to formulate a general understanding into the strength of the different possible decay rates in the nanogaps, we began by comparing the total decay rate enhancements (Purcell factor) $F_P = \frac{\Gamma_T}{\Gamma_0}$ to the radiative decay rate enhancements $\frac{\Gamma_{rad}}{\Gamma_0}$ for a z -field oscillating dipole located at the centre of a nanogap. Taking a gap of width $d = 28$ nm between a 100 nm silver particle and a 100 nm thick extended silver film, we present this as a function of free space wavelength. Figure 2 summarises these results. The enhancements in $\frac{\Gamma_T}{\Gamma_0}$ can be divided into two regions; region I spans the wavelength range from 350 nm to 500 nm and peaks at approximately 400 nm, close to the surface plasmon resonance (SPR) of a planar silver film.⁹ Region II consists of a broad enhancement peak that covers the spectral range between 500 nm and 1000 nm and peaks close to 570 nm. By comparing $\frac{\Gamma_T}{\Gamma_0}$ to $\frac{\Gamma_{rad}}{\Gamma_0}$, it becomes clear that the enhancements in Γ_T in region I are mainly dominated by Ohmic losses by the metal, while the enhancements in Γ_T in region II are mainly dominated by radiative decay rate enhancements. From this

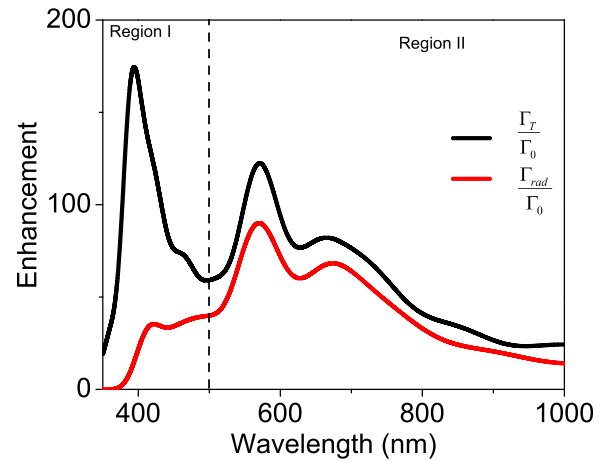


FIG. 2. The calculated enhancements in the total decay rate (Purcell factor) and the radiative emission rate from a nanogap of width 28 nm formed between a silver nanoparticle of diameter of a 100 nm and an extended film thickness of 100 nm.

observation, we conclude that region II is well suited for applications which require enhancements in the radiative emission rate of a broad emission bandwidth emitter. Further, simulations were carried out to briefly study the effects of changing the metal structures from silver to gold. It is previously known that both the SPR of a planar film and the local SPR of gold nanostructures are at a longer wavelength to that of silver.³⁹ The simulation results agree with this and again show similar effects and regions of enhancement to that of silver, albeit at longer wavelengths. Region I dominated by Ohmic losses peaks at 530 nm, close to the SPR of a gold planar film³⁹ and region II consisting of broad twin peaks at 620 nm and 710 nm. Region II again is dominated mainly by radiative decay rate enhancements and would be suitable for similar broadband emitters between 600 nm and 1000 nm. From the above discussion, it is clear that the spectral position of region I is mainly determined by the nature of the plasmonic material used.

Figure 3 illustrates the electric field amplitude $|E|$ and its real z -component (E_z) at the wavelength of the peak position of region I ($\lambda = 394$ nm), peak position of region II ($\lambda = 570$ nm), and at shoulder of region II ($\lambda = 676$ nm). In all cases, the field is strongly localised and enhanced within the nanogap. The field distribution at the peak position of region I has a narrow spatial distribution with the field maximum close to the metal surfaces. However, the field distribution at the peak position of region II extends laterally to around ~ 100 nm with a field maximum close the silver nanoparticle surface. In all cases, the field amplitude $|E|$ consists of two lateral lobes, one above the nanoparticle and the other below the nanoparticle, which indicate that plasmonic modes excited in the nanoparticle are associated with dipole moments perpendicular to the planar silver film.⁴⁰

From the enhancements in region II, we deduced a Purcell factor of $F_P = \frac{\Gamma_T}{\Gamma_0} = 58$, radiative decay rate enhancements of $\frac{\Gamma_{rad}}{\Gamma_0} = 45$ times yielding a quantum efficiency of $\phi_m = 0.77$ from the emitter-nanogap system and a mode volume $V = 0.02 \left(\frac{\lambda}{2n}\right)^3$ almost 50 times smaller than the diffraction limit. The Purcell factor and the quantum efficiency

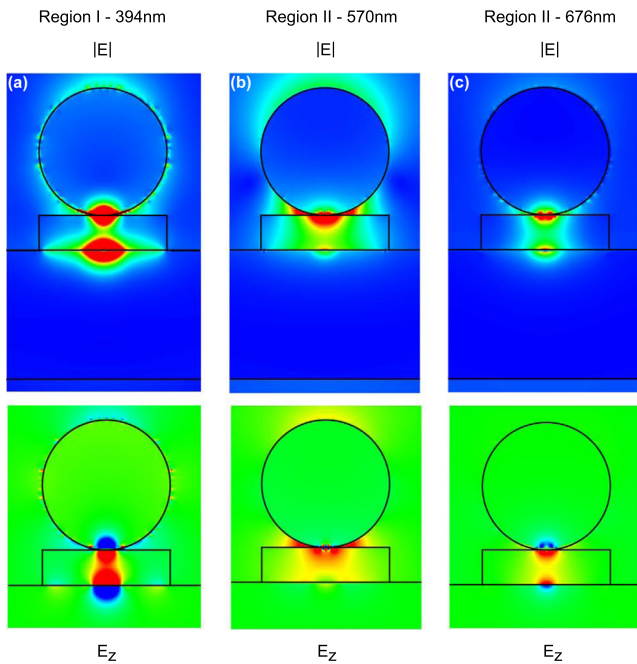


FIG. 3. The magnitude of the total electric field ($|E|$) and the real part of the z-component of the field within the nanogap at wavelengths (a) 394 nm, (b) 570 nm, and (c) 676 nm. Part (a) corresponds to the peak enhancement of region I, part (b) to the peak enhancement of region II, and part (c) corresponds to the shoulder of region II. It should be noted that the fields in part (c) are scaled up by a factor of 2 relative to the fields in part (a) and (b).

predicted in this work are almost two times higher than those predicted by Esteban *et al.*¹¹ from silver based optical patch antennas. For comparison, we also calculated the enhancements in the radiative decay rate $\frac{\Gamma_{rad}}{\Gamma_0}$ from a similar nanogap formed between a 100 nm diameter silver cylinder with its major axis perpendicular to the plane and an extended silver film. The calculations showed that the enhancements from the sphere based nanogap are 1.25 to 1.7 times higher than the enhancements from a 100 nm diameter disk of heights ranging between 100 nm and 20 nm. The physical reason for this would appear to stem from the loss in symmetry in the structure and the different modes associated with the cylinder do not align with the fields from the z-oriented dipole.

The relative contribution of the radiative decay rate and the nonradiative decay rate into the total enhancement in the decay rate depends on the distance between the emitting dipole and the plasmonic nanostructure. This distance determines if the dipole is coupled to far field radiation or absorbed nonradiatively by the metal. Therefore, by varying the gap width d , the interplay between the radiative decay rate and the nonradiative decay rate can be controlled. Figure 4 shows a systematic comparison of Γ_T and Γ_{rad} for a gap of width d varying between 12 nm and 60 nm formed between a 100 nm silver particle and a 100 nm thick extended silver film. In the calculations, we placed the dipole at the centre of the gap and assumed the intrinsic quantum efficiency of the emitting dipole is 1. In particular, we plot Γ_T (black line) and Γ_{rad} (red line) integrated over the spectral range of region I and II (350 nm to 1000 nm) along with Γ_{TII} (green line) and Γ_{radII} (blue line) integrated over the spectral range of region II (500 nm to 1000 nm). For comparison, we also plot the enhancements in Γ_{rad} (orange line)

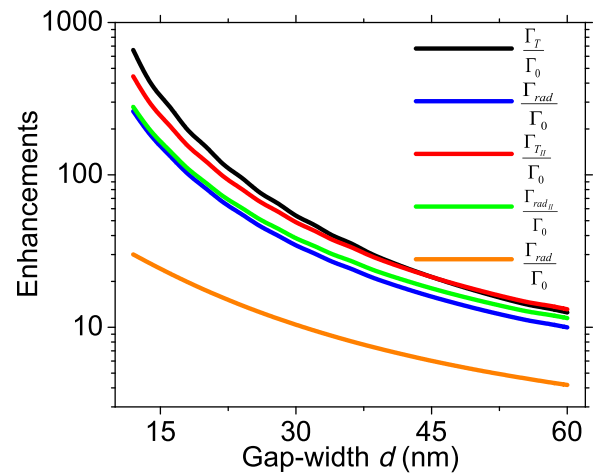


FIG. 4. Calculated enhancements in $\frac{\Gamma_T}{\Gamma_0}$ (black line), $\frac{\Gamma_{rad}}{\Gamma_0}$ (blue line), $\frac{\Gamma_{TII}}{\Gamma_0}$ (red line), and $\frac{\Gamma_{radII}}{\Gamma_0}$ (green line) as a function of the gap-width d for a nanogap of $D = 100$ nm and $t = 100$ nm. For comparison, we also plot the enhancements in radiative decay rate of a single sphere of diameter a 100 nm placed at a distance d from a z-polarised oscillating dipole (orange line).

from a structure without the extended silver film. As it can be seen, both Γ_T and Γ_{rad} drop rapidly with increasing gap width d , as expected² and for all values of d , Γ_{radII} is greater than Γ_{rad} . Furthermore, for gap widths between 12 nm and 25 nm, 60% to 43% of the enhancements in Γ_T stem from Ohmic losses by the metal. On the contrary, when we consider the enhancements in Γ_{TII} over the same gap width range, we find that only 30% of the enhancements in Γ_{TII} are due to Ohmic losses by the metal. Recently, Chen *et al.*⁴¹ theoretically investigated the enhancements in the radiative decay rate using a nanogap. This was formed between a metallic nanoparticle and a planar dielectric layer and studied as a function of the refractive index the dielectric layer. For a dielectric layer of refractive index of 1.5 mimicking an organic host matrix, the predicted enhancements are of the same order to what we predicted in this work from a structure without the extended silver film (see Fig. 4). However, the quantum efficiency for such system is only 0.3, almost half of what we predicted by placing the emitting dipole into a plasmonic cavity. Another fundamental difference between our design and the one proposed by Chen *et al.* is that our design is able to enhance the decay rate over the whole visible range while the one proposed by Chen *et al.* is only limited to a 100 nm bandwidth.

In the calculations presented in Fig. 4, we assumed that $\phi_0 = 1$, however for many organic molecules $\phi_0 < 1$. To get further insight into the relative contribution of Γ_{radII} and Γ_{nrII} into the emitter-nanogap system, we used the results in Figure 3 and Eq. (3) to relate the quantum efficiency of the emitter-nanogap system ϕ_m into the intrinsic quantum efficiency ϕ_0 of the emitting dipole as a function of the gap width d . In Fig. 5(a), we plot ϕ_m integrated over the spectral range of region II as a function of ϕ_0 and d for a gap formed between a 100 nm silver particle and a 100 nm thick extended silver film. The dependence of ϕ_m on ϕ_0 and d can be split into three distinctive regions. First region applies for $\phi_0 < 0.08$. In this region, ϕ_m decreases with increasing d as illustrated in Fig. 5(b). Therefore, for applications

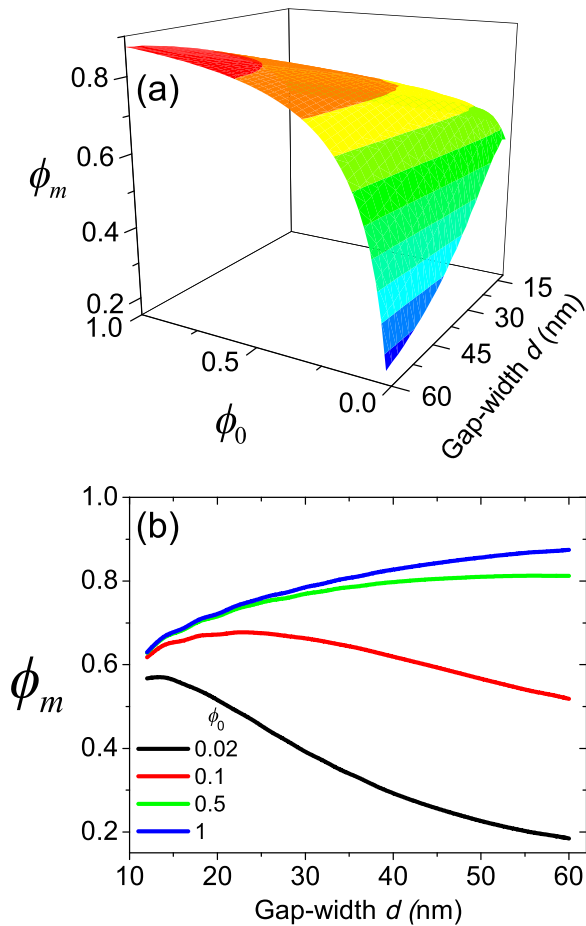


FIG. 5. Part (a) shows the calculated emitter-nanogap quantum efficiency ϕ_m as a function of the intrinsic quantum efficiency ϕ_0 and the gap-width d for a nanogap of $D = 100$ nm and $t = 100$ nm. Part (b) shows the calculated emitter-nanogap quantum efficiency ϕ_m as a function of the gap-width d for different values of ϕ_0 .

involving the use of very low quantum efficiency emitting materials, a small gap width has to be used. For example, poly(3-hexylthiophene) P3HT, has $\phi_0 = 0.02$,⁴² thus ϕ_m can be as high as 0.57 using a nanogap of width 12 nm with 30-fold enhancements in the quantum efficiency. Our predicted enhancements are 10 times higher than those predicted by O'Carroll *et al.*⁴³ using a single nanowire antenna. The second region applies for $0.08 < \phi_0 < 0.4$. In this region, at the beginning ϕ_m increases with increasing d to reach a maximum value then drops with further increasing of d as can be seen in Figure 5(b). The observed behaviour of ϕ_m with ϕ_0 and d in the first and second region depends on the interplay between the values of $\frac{\Gamma_{TII}}{\Gamma_0}$, $\frac{\Gamma_{radII}}{\Gamma_0}$, and $\frac{k_{av}}{\Gamma_0}$. The third region applies for $\phi_0 > 0.4$, where ϕ_m increases with increasing d as can be seen in Fig. 5(b). In this region, the behaviour of ϕ_m against ϕ_0 and d can be understood as follows; for $\phi_0 > 0.4$, the term $\frac{k_{av}}{\Gamma_0}$ is very small compared to the term $\frac{\Gamma_{TII}}{\Gamma_0}$ and thus can be ignored; therefore, the behaviour of ϕ_m is predominantly controlled by the term $\frac{\Gamma_{radII}}{\Gamma_{TII}}$, which increases with increasing d . This is a result of the reduction in the Ohmic losses with increasing d . Another interesting finding is that for intrinsic quantum efficiency ϕ_0 less than 0.62, the quantum efficiency of the emitter-nanogap system ϕ_m is larger or equal to ϕ_0 for all values of d .

Next, we study the enhancements in Γ_{TII} and Γ_{radII} as a function of the size of the silver nanoparticle D . In these calculations, we fixed the gap width at a value of $d = 28$ nm and the thickness of the extended silver film at $t = 100$. In Fig. 6(a), we plot the enhancements in Γ_{TII} (black line) and Γ_{radII} (red line) integrated over the spectral range of region II as a function of the nanoparticle size D . The enhancements in both Γ_{TII} and Γ_{radII} increase strongly with increasing D and peak around $D \sim 180$ nm, then drop slightly for $D > 180$ nm. To get further insight into the origin of this behaviour, we plot in Fig. 6(b) the enhancements in Γ_T (Purcell factor) versus free space wavelength for a gap of width $d = 28$ nm formed using particles of size 30 nm, 120 nm, and 180 nm. For a particle of diameter $D = 30$ nm, the enhancements in Γ_T are predominantly located in region I, close to the surface plasmon resonance of a planar silver film. With increasing D , enhancements in region II start to evolve as illustrated in Fig. 6(b). These results are in agreement with the work of Chowdhury *et al.*⁴⁴ and Jun *et al.*⁹ who attributed the evolution of region II with increasing the particle size to higher order enhancement modes⁴⁵ and to tight confinements of the modes within the cavity.⁹ In addition, the peak position of region II shifts to a longer wavelength with increasing D as expected from a circular cavity.⁴⁶ For our spectral range of interest, enhancements in region II take their maximum value at $D \sim 180$ nm.

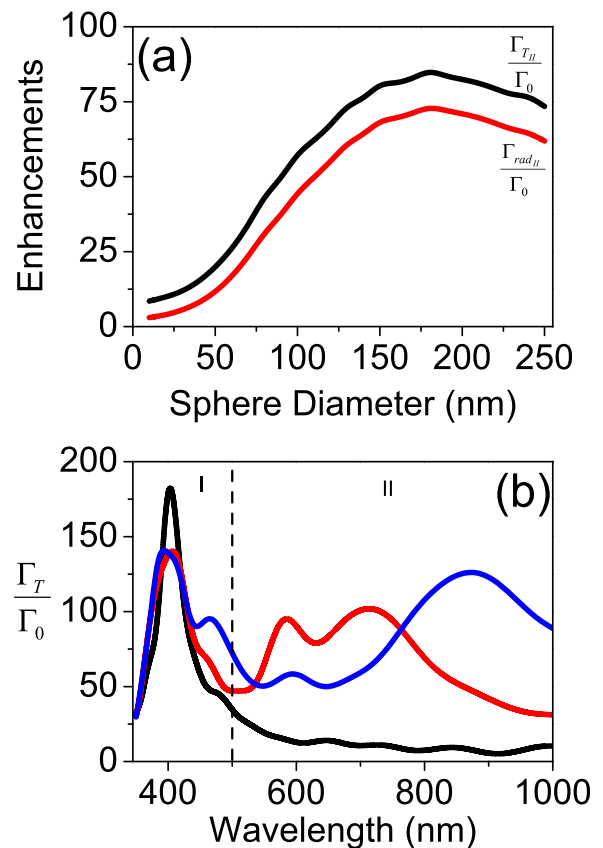


FIG. 6. Part (a) shows $\frac{\Gamma_{TII}}{\Gamma_0}$ (black line) and $\frac{\Gamma_{radII}}{\Gamma_0}$ (red line) as a function of the silver nanoparticle diameter D for a nanogap of $d = 28$ nm and $t = 100$ nm. Part (b) shows $\frac{\Gamma_T}{\Gamma_0}$ as a function of the vacuum wavelength for a gap of width $d = 28$ nm, a diameter $D = 30$ nm (black line), $D = 120$ nm (red line) and $D = 180$ nm (blue line), and $t = 100$ nm.

So far, we have investigated the dependence of the enhancements of the spontaneous emission rate on the gap-width d and particle size D . Another parameter that could potentially influence the enhancements of Γ_{TII} and Γ_{radII} , is the thickness of the extended silver film t . Our calculations showed that both Γ_{TII} and Γ_{radII} have no clear dependence on t illustrating the near field nature of the field enhancements of the system. However, changing t allows us to manipulate the ratio between the light emitted in forward direction relative to the light emitted in backward direction.

Up to now, in all our calculations, we placed the emitting dipole at the nanogap centre, however the relative contribution of the radiative decay rate and the nonradiative decay rate into the total enhancement of the decay rate depends on the vertical position z of the emitting dipole. To investigate this effect, we calculate the Purcell factor $\frac{\Gamma_{TII}}{\Gamma_0}$ and enhancements in the radiative decay rate $\frac{\Gamma_{radII}}{\Gamma_0}$ integrated over the spectral range of region II as a function of the dipole position z for a nanogap of width 28 nm formed between a silver sphere of diameter $D = 100$ nm and a 100 nm extended silver film. The results of these calculations are illustrated in Fig. 7(a). The dependence of $\frac{\Gamma_{TII}}{\Gamma_0}$ on z takes the form of an asymmetric U shape around $z = 0$. This stems from the asymmetric nature of the investigated structure around the $z = 0$ plane (see Fig. 1). On the other hand, $\frac{\Gamma_{radII}}{\Gamma_0}$ increases with increasing z . To quantify the relation between the radiative decay rate and the nonradiative decay rate with the position of the emitting dipole, we plot in Fig. 7(b) the relation

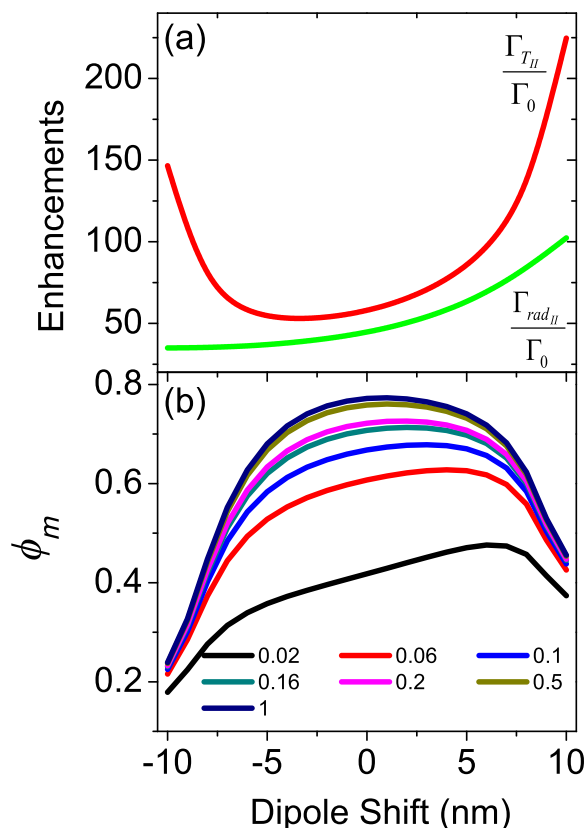


FIG. 7. Part (a) shows $\frac{\Gamma_{TII}}{\Gamma_0}$ (red line) and $\frac{\Gamma_{radII}}{\Gamma_0}$ (green line) as a function of the dipole position z in a nanogap of $d = 28$ nm, $D = 100$ nm, and $t = 100$ nm. Part (b) shows the calculated emitter-nanogap quantum efficiency ϕ_m as a function of the dipole position z for different values of ϕ_0 .

between ϕ_m as a function of z for different values of ϕ_0 . For materials of $\phi_0 > 0.26$, ϕ_m peaks at $z = 1$ nm, with less than 12% variation in ϕ_m within the 10 nm central region. For materials of $\phi_0 < 0.26$, ϕ_m peaks around $z \sim 5$ nm with a steep variation in ϕ_m with increasing z within the 10 nm central region as can be seen in Figure 7(b). The results in Fig. 7(b) suggest that for materials of low quantum efficiency $\phi_0 < 0.26$, it is important to position the emitting material 5 nm above the gap centre to optimise the quantum efficiency. For materials of $\phi_0 > 0.26$, the optimum position for locating the active material is at the centre of the nanogap.

IV. CONCLUSION

In conclusion, we have used FDTD calculations to model the optical modifications in the spontaneous emission rate and the quantum efficiency of an emitting dipole placed within a plasmonic nanogap. The nanogap is formed between a silver nanoparticle and an extended silver film and the optical modifications are presented as a function of the gap geometrical parameters. Over 100 times enhancements in the radiative spontaneous emission rate combined with a mode volume of $0.02(\frac{\lambda}{2n})^3$ (almost 50 times smaller than the diffraction limit) can be achieved over the whole visible range using realistic geometrical parameters. Further to that, our calculations showed that a plasmonic nanogap of width 18 nm formed between a 100 nm silver nanoparticle and an extend silver film provides 110 times enhancement in the radiative emission rate of materials of intrinsic quantum efficiency in the range of $0.7 \geq \phi_0 \geq 0.02$. This is combined with 1 to 27 times enhancements in the quantum efficiency. Our calculations indicate the same gap provides over 110-fold enhancements in the radiative emission rate of materials of intrinsic quantum efficiency $\phi_0 \geq 0.7$ while maintaining a quantum efficiency of about 0.71 over the whole visible range. These structures are of great interest for both fundamental light matter interaction studies and potential applications in quantum optics and Raman spectroscopy.

ACKNOWLEDGMENTS

We thank Arthur Thijssen for providing us of his modified version of Meep and Angela Dyson for helpful discussions and comments on the manuscripts. AE would like to thank the University of Hull for the award of a PhD studentship.

- ¹A. V. Akimov, A. Mukherjee, C. L. Yu, D. E. Chang, A. S. Zibrov, P. R. Hemmer, H. Park, and M. D. Lukin, *Nature* **450**, 402–406 (2007).
- ²D. E. Chang, A. S. Sørensen, P. R. Hemmer, and M. D. Lukin, *Phys. Rev. Lett.* **97**, 053002 (2006).
- ³S. Kumar, A. Huck, and U. L. Andersen, *Nano Lett.* **13**, 1221 (2013).
- ⁴E. Stock, F. Albert, C. Hopfmann, M. Lerner, C. Schneider, S. Höfling, A. Forchel, M. Kamp, and S. Reitzenstein, *Adv. Mater.* **25**, 707 (2013).
- ⁵S. Noda, M. Fujita, and T. Asano, *Nat. Photonics* **1**, 449 (2007).
- ⁶E. J. R. Vesseur, F. J. García de Abajo, and A. Polman, *Phys. Rev. B* **82**, 165419 (2010).
- ⁷K. J. Russell, T.-L. Liu, S. Cui, and E. L. Hu, *Nat. Photonics* **6**, 459 (2012).
- ⁸L. A. Blanco and F. J. García de Abajo, *Phys. Rev. B* **69**, 205414 (2004).
- ⁹Y. C. Jun, R. D. Kekatpure, J. S. White, and M. L. Brongersma, *Phys. Rev. B* **78**, 153111 (2008).

- ¹⁰V. G. Kravets, G. Zorinians, C. P. Burrows, F. Schedin, C. Casiraghi, P. Klar, A. K. Geim, W. L. Barnes, and A. N. Grigorenko, *Phys. Rev. Lett.* **105**, 246806 (2010).
- ¹¹R. Esteban, T. V. Teperik, and J. J. Greffet, *Phys. Rev. Lett.* **104**, 026802 (2010).
- ¹²K. Tanaka, E. Plum, J. Y. Ou, T. Uchino, and N. I. Zheludev, *Phys. Rev. Lett.* **105**, 227403 (2010).
- ¹³A. Kinkhabwala, Z. Yu, S. Fan, Y. Avlasevich, K. Müllen, and W. E. Moerner, *Nat. Photonics* **3**, 654–657 (2009).
- ¹⁴E. M. Purcell, *Phys. Rev.* **69**, 681 (1946).
- ¹⁵M. Boroditsky, R. Vrijen, T. F. Krauss, R. Coccioli, R. Bhat, and E. Yablonovitch, *J. Lightwave Technol.* **17**, 2096 (1999).
- ¹⁶S. Noda, *J. Lightwave Technol.* **24**, 4554 (2006).
- ¹⁷T. van der Sar, J. Hagemeyer, W. Pfaff, E. C. Heeres, S. M. Thon, H. Kim, P. M. Petroff, T. H. Oosterkamp, D. Bouwmeester, and R. Hanson, *Appl. Phys. Lett.* **98**, 193103 (2011).
- ¹⁸J. G. Müller, U. Lemmer, G. Raschke, M. Anni, U. Scherf, J. M. Lupton, and J. Feldmann, *Phys. Rev. Lett.* **91**, 267403 (2003).
- ¹⁹Z. Yu and P. F. Barbara, *J. Phys. Chem. B* **108**, 11321 (2004).
- ²⁰J. R. Buck and H. J. Kimble, *Phys. Rev. A* **67**, 033806 (2003).
- ²¹Y. Zhang and M. Lončar, *Opt. Lett.* **34**, 902 (2009).
- ²²M. Lerner, N. Gregersen, F. Dunzer, S. Reitzenstein, S. Höfling, J. Mørk, L. Worschech, M. Kamp, and A. Forchel, *Phys. Rev. Lett.* **108**, 057402 (2012).
- ²³Y. Ota, M. Shirane, M. Nomura, N. Kumagai, S. Ishida, S. Iwamoto, S. Yorozu, and Y. Arakawa, *Appl. Phys. Lett.* **94**, 033102 (2009).
- ²⁴S. Haddadi, L. Le-Gratiet, I. Sagnes, F. Raineri, A. Bazin, K. Bencheikh, J. A. Levenson, and A. M. Yacomotti, *Opt. Express* **20**, 18876 (2012).
- ²⁵P. Bharadwaj, B. Deutsch, and L. Novotny, *Adv. Opt. Photonics* **1**, 438 (2009).
- ²⁶K. J. Russell, K. Y. M. Yeung, and E. Hu, *Phys. Rev. B* **85**, 245445 (2012).
- ²⁷S. Schietinger, M. Barth, T. Aichele, and O. Benson, *Nano Lett.* **9**, 1694 (2009).
- ²⁸M. A. Noginov, G. Zhu, A. M. Belgrave, R. Bakker, V. M. Shalaev, E. E. Narimanov, S. Stout, E. Herz, T. Suteewong, and U. Wiesner, *Nature* **460**, 1110 (2009).
- ²⁹R.-M. Ma, R. F. Oulton, V. J. Sorger, G. Bartal, and X. Zhang, *Nat. Mater.* **10**, 110 (2011).
- ³⁰M. Kuttge, F. J. Garcia de Abajo, and A. Polman, *Nano Lett.* **10**, 1537 (2010).
- ³¹M. H. Chowdhury, J. Pond, S. K. Gray, and J. R. Lakowicz, *J. Phys. Chem. C* **112**, 11236 (2008).
- ³²O. L. Muskens, V. Giannini, J. A. Sánchez-Gil, and J. Gómez Rivas, *Nano Lett.* **7**, 2871 (2007).
- ³³V. G. Kravets, G. Zorinians, C. P. Burrows, F. Schedin, A. K. Geim, W. L. Barnes, and A. N. Grigorenko, *Nano Lett.* **10**, 874 (2010).
- ³⁴A. F. Oskooi, D. Roundy, M. Ibanescu, P. Bermel, J. D. Joannopoulos, and S. G. Johnson, *Comput. Phys. Commun.* **181**, 687 (2010).
- ³⁵F. Kaminski, V. Sandoghdar, and M. Agio, *J. Comput. Theor. Nanosci.* **4**, 635 (2007).
- ³⁶Y. Xu, J. S. Vučković, R. K. Lee, O. J. Painter, A. Scherer, and A. Yariv, *J. Opt. Soc. Am. B* **16**, 465 (1999).
- ³⁷A. Vial, A.-S. Grimault, D. Macías, D. Barchiesi, and M. L. De la Chapelle, *Phys. Rev. B* **71**, 085416 (2005).
- ³⁸A. D. Rakic, A. B. Djuricic, J. M. Elazar, and M. L. Majewski, *Appl. Opt.* **37**, 5271 (1998).
- ³⁹J. J. Mock, R. T. Hill, A. Degiron, S. Zauscher, A. Chilkoti, and D. R. Smith, *Nano Lett.* **8**, 2245 (2008).
- ⁴⁰Y. Wu and P. Nordlander, *J. Phys. Chem. C* **114**, 7302 (2010).
- ⁴¹X.-W. Chen, M. Agio, and V. Sandoghdar, *Phys. Rev. Lett.* **108**, 233001 (2012).
- ⁴²N. C. Greenham, I. D. W. Samuel, G. R. Hayes, R. T. Phillips, Y. A. R. R. Kessener, S. C. Moratti, A. B. Holmes, and R. H. Friend, *Chem. Phys. Lett.* **241**, 89 (1995).
- ⁴³D. M. O'Carroll, C. E. Hofmann, and H. A. Atwater, *Adv. Mater.* **22**, 1223 (2010).
- ⁴⁴M. H. Chowdhury, K. Ray, M. L. Johnson, S. K. Gray, J. Pond, and J. R. Lakowicz, *J. Phys. Chem. C* **114**, 7448 (2010).
- ⁴⁵G. Sun and J. B. Khurgin, *Appl. Phys. Lett.* **98**, 113116 (2011).
- ⁴⁶S.-H. Kwon, *Opt. Express* **20**, 24918 (2012).